

A Novel Low-Profile Phased Antenna With Dual-Port and Its Application in 1-D Linear Array to 2-D Scanning

Kun Wang¹, Junping Geng¹, *Senior Member, IEEE*, Han Zhou¹, Silei Yang, Rui Zhao, Jie Chen¹,
Jingzheng Lu, Xudong Tang¹, Jing Zhang, and Ronghong Jin¹, *Fellow, IEEE*

Abstract—A novel low-profile phased antenna with dual-port and its two types of 1-D linear array to 2-D space wide-angle beam scanning are proposed. The antenna unit is composed of fishbone structure and rhombus parasitic patch, which is folded into n-shaped to low profile 0.08λ . By adjusting the phase difference ($\Delta\varphi$) from 0° to 180° , the antenna working mode is changed from even mode to hybrid mode and to odd mode eventually. Therefore, the proposed antenna unit realizes wide-angle scanning characteristics and continuous switching state from broadside lobe to endfire lobe. Furthermore, the proposed phased antenna element is extended to two kinds of 1-D linear phased array (Array#1 and Array#2) based on the generalized principle of the pattern multiplication. The fabricated Array#1 can realize beam scanning range $-116^\circ < \theta_m < 0^\circ$ (xoz plane), $0^\circ < \theta_m < 63^\circ$ ($yozy$ plane), and $90^\circ < \Phi_m < 169^\circ$ (xoy plane) and the fabricated Array#2 can achieve $0^\circ < \theta_m < 60^\circ$ (xoz plane), $0^\circ < \theta_m < 65^\circ$ ($yozy$ plane), and $90^\circ < \Phi_m < 152^\circ$ (xoy plane). The proposed phased antenna unit and its 1-D array can realize 2-D space wide-angle scanning, improving scanning performance and expanding scanning dimensional space in phased array.

Index Terms—1-D linear array, 2-D space wide-angle scanning, generalized principle of the pattern multiplication (GPPM), phased antenna unit, phased array.

I. INTRODUCTION

PHASED arrays have broad application prospects in wireless communication technology, such as system capacity increasement, spectrum efficiency improvement, channel anti-interference ability enhancement, and beamforming. In particular, its flexible continuous beam scanning and high-gain characteristics are widely used in wide-angle scanning such as radar, satellite, wireless communication systems, and other application scenarios, especially in high-speed moving equipment, which has an urgent need for the phased array with

low-profile, high-gain, and multidimensional space scanning characteristics [1]–[5].

Generally, the phased array has the advantages of wide-angle scanning and high gain [6], [7]. Nevertheless, it has some problems. For example, the mutual coupling among antenna unit limits the scanning range, the active impedance mismatch leads to gain roll-off in the process of wide-angle scanning, and the traditional linear array only realizes beam scanning characteristic in the 1-D space [8]–[12].

In general, the wide-beam antenna unit can effectively improve the wide-angle scanning performance of the phased array [13]–[17]. In the previews report [18], the planar linear array based on the wide-beam antenna unit could realize the wide-angle scanning characteristics from the broadside direction to the endfire direction (-89° to 90° in the H-plane).

Usually, the conventional linear array can only scan in the 1-D space, and the 2-D space scanning can be realized by 2-D array or multidimensional array, that is to say, it is a challenge to realize high radiation performance in the finite space of the wireless systems.

The antenna unit based on the reconfigurable technology can adjust the surface current distribution, to exchange its resonance mode and obtain the multibeam characteristic. Actually, the switching characteristics of the reconfigurable network mainly depend on the ON-state or OFF-state of the p-i-n diodes. Also, the characteristics of the p-i-n diode affect switching time and electromagnetic signature of the reconfigurable network, which limits the scanning performance of the reconfigurable antenna [19]–[21], and may worsen the radiation performance of the antenna. Furthermore, the complex reconfigurable network takes up lots of the system spaces, which brings the problems of the system miniaturization and noise [22], [23].

In recent years, leaky-wave antennas have attracted attention due to low cost, frequency beam scanning [24]–[27], and compact structure. In general, the electromagnetic energy of the leaky-wave antenna propagates in one direction, by adjusting the phase constant and the periodic structure to realize the energy is being leaked and radiated from the slot structure [28]–[32]. The spoof surface plasmon polaritons (SSPPs) structures are widely used in microwave equipment, such as antennas [35], [36], filters [37], [38], and metasurface [39]. To improve the performance of the wide-angle beam scanning,

Manuscript received 29 October 2021; revised 15 February 2022; accepted 27 February 2022. Date of publication 28 March 2022; date of current version 8 September 2022. This work was supported by the National Natural Science Foundation under Grant 61571289, Grant 61571298, and Grant 61471240. (Corresponding author: Junping Geng.)

Kun Wang, Junping Geng, Han Zhou, Silei Yang, Rui Zhao, Jingzheng Lu, Xudong Tang, Jing Zhang, and Ronghong Jin are with the Department of Electronics Engineering, Shanghai Jiao Tong University, Shanghai 200240, China (e-mail: gengjup@sjtu.edu.cn).

Jie Chen is with the China Ship Development and Design Center, Wuhan 430060, China.

Color versions of one or more figures in this article are available at <https://doi.org/10.1109/TAP.2022.3161339>.

Digital Object Identifier 10.1109/TAP.2022.3161339

the dual-port antenna represented by the SSPPs structure in the leaky-wave antenna shows great potential [33]. The basic operating mode of the SSPPs' antenna includes the even mode and odd mode while showing the broadside lobe and the endfire lobe characteristics, respectively [34]. Generally, the one feed port SSPPs' antenna mainly excites a single working mode at a given frequency. In order to achieve new operating modes to obtain multibeam scanning characteristics, the reconfigurable network is introduced to adjust the beam direction of the SSPPs' antenna. When switching the reconfigurable network state, the surface current phase of the SSPPs' antenna changes, and its radiation patterns also change accordingly [34]. However, the parasitic radiation effects, RF-link insertion loss [40], and limited switching states of the reconfigurable network all limit the performances of the reconfigurable antenna.

For conventional phased array, beam scanning characteristics mainly depend on the array layout method, array factor function, and other parameters, while the element factor in the traditional array wide-angle scanning is almost negligible.

In the previous study [41], [42], the generalized principle of pattern multiplication (GPPM) is proposed based on the generalized element factor (GEF). Also, the GEF is realized by the phase mode antenna (PMA) with dual-port, and the PMA can scan with the different phase difference between dual-port. Thus, the generalized array with PMA can scan more wide-angle range and further realize 2-D or multidimensional scanning characteristics with 1-D PMA array by two-stage phase control.

In the previews report [43], the dual-port antenna unit based on the SSPPs structure is excited for lobe scanning in the 2-D space. By adjusting the phase difference between the dual-port feeding, the odd mode and even mode of the antenna are superimposed to achieve hybrid mode. Accordingly, continuous beam scanning from the endfire to the broadside radiation lobe is performed. Furthermore, the two linear arrays based on this PMA element are constructed and change the array factor and the element factor of 1-D linear array, in order to realize the beam scans in the θ -direction and the Φ -direction, respectively. The 2-D space scanning characteristics are achieved by the 1-D line array, which shows good beam scanning performance. One thing to note is that the profile of the antenna unit is about 0.7λ , which is too high for equipment with low profile and conformal, and the scanning range and performance of the array should still be further optimized.

In order to realize the low-profile phased antenna, expand the beam scanning range, and optimize the array scanning performance in 2-D space, a dual-port phased antenna with low-profile fishbone structure and its two kinds of 1-D linear array are proposed. The designed low-profile antenna unit can work in odd mode, even mode, and hybrid modes by adjusting the phase difference ($\Delta\varphi$) between two feed ports. It can be seen that, with $\Delta\varphi$ between the dual-port of the antenna unit changing, the main lobe direction varies from the endfire lobe to the broadside lobe (about 0° to -68°). In addition, two kinds of 1-D linear array are proposed based on the proposed phased antenna unit and the GPPM. Finally, considering the antenna elements layout method, the GEF function and the generalized array factor (GAF) function are achieved to realize

the 2-D space wide-angle scanning characteristics in Array#1 and Array#2.

The experimental results show that the fabricated Array#1 can realize about $\pm 116^\circ$ wide-angle beam scanning along the θ -direction (xoz plane) with gains of about 6.9–11.7 dBi, $\pm 63^\circ$ wide-angle beam scanning along the θ -direction (yo z plane) with gains of about 11.7–6.7 dBi, and 90° – 169° wide-angle beam scanning along the Φ -direction (xoy plane) with gains about 6.2–4.4 dBi. Meanwhile, the proposed Array#2 can obtain $\pm 60^\circ$ wide-angle beam scanning along the θ -direction (xoz plane) with gains of about 7–12 dBi, $\pm 65^\circ$ wide-angle beam scanning along the θ -direction (yo z plane) with gains of about 11.9–7.6 dBi, and 90° – 152° wide-angle beam scanning along the Φ -direction (xoy plane) with gains of about 7.3–4 dBi.

The remainder of this article is organized as follows. Section II illustrates the proposed antenna structure, operating principle, key parameters analysis, and measured results analysis. Section III shows the proposed two kinds of 1-D linear array prototype and experimental results. Finally, the conclusion is given in Section IV.

II. ANTENNA ANALYSIS AND DESIGN

A. Antenna Configuration

The top view and side view of the proposed phased antenna unit based on fishbone structure are shown in Fig. 1(a) and (b), respectively. The radiation patch of the proposed phased antenna unit mainly consists of an H-shaped fishbone structure and a rhombus parasitic patch, which all are sheet copper ($th_1 = 2$ mm). The fishbone structure looks like a very short "n" with the length of the metal arms l , the length in the x -direction d , the gap s , and the profile height is h . Here, the length l of the metal arms mainly affects the operating resonant frequency, but the length d is not sensitive for the working resonant frequency and the bandwidth. We set the original value of $l = 45$ mm and miniaturized d to 26 mm.

Meanwhile, the gap s between the metal arms in the fishbone structure mainly affects the coupling strength, and the width p of the metal arms can appropriately improve the working bandwidth. The profile height h of fishbone structure is 10 mm, about 0.08λ , and the low-profile configuration is conducive to the miniaturization of the system. The main axis width w_2 in the fishbone structure undertakes for the stability of the entire antenna structure, which is set 6 mm. In order to enhance the radiation performance of the antenna unit, a rhombus parasitic patch ($m \times n$) is introduced in the center of fishbone structure. As the phased antenna, the surface current phase distribution of the antenna unit is adjusted and controlled by $\Delta\varphi$ between the dual-port. Thus, there are two tuning stubs (w_1) being added on the surface of the fishbone's metal arms, which are used as Ports 1 and 2 feeding. On another side, the ground (GND) ($th_3 = 4$ mm) is mainly used for the installation of the proposed antenna and SMA connector. To avoid that fishbone structure might be shorted to the GND, one substrate ($th_2 = 1.524$ mm, $\epsilon_r = 2.5$, and $\delta = 0.0013$) is placed between the proposed antenna unit and the GND. Finally, the substrate and the GND are fixed by four screws.

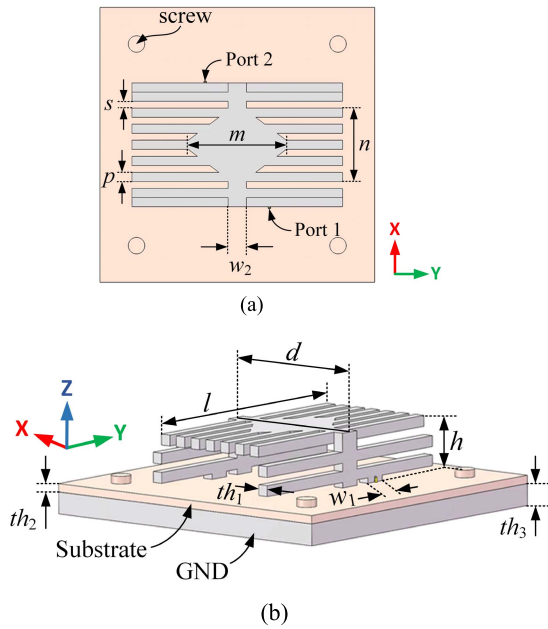


Fig. 1. Configuration of the proposed antenna unit. (a) Top view. (b) Side view.

B. Working Principle of the Proposed Antenna Unit

As shown in Fig. 1(a), the two feed ports of the proposed antenna unit can be fed with equal amplitude and arbitrary phase difference in the range of 0° – 180° , where the phase of each feed port is defined as φ_1 (Port 1) and φ_2 (Port 2). Thus, the phase difference between the two feed ports is shown as $\Delta\varphi = \varphi_2 - \varphi_1$.

As mentioned above, the proposed phased antenna unit is based on the fishbone structure, which can work in the odd mode or even mode as the leaky-wave antenna. When the phase difference $\Delta\varphi$ between the two feed ports is changed, the working modes of the proposed phased antenna vary from odd mode to hybrid mode and then to even mode.

1) E_y Component Varying With the Phase Difference $\Delta\varphi$: The simulated E_y component distribution (yoz plane) of the proposed antenna unit is shown in Fig. 2. The cross section of the proposed antenna unit in the yoz plane is divided into four quadrants (I–IV), the front view is shown in Fig. 2(a), and the side view is shown in Fig. 2(b).

When only one port, either Port 1 or Port 2 is excited, the E_y component distribution (yoz plane) is shown in Fig. 2(c). Meanwhile, the antenna mainly excites the odd-mode characteristic in the left part, and the E_y component distribution is mainly focused on the second quadrant (II). It means that the surface currents distribution is mainly on the left arms along the y -axis.

As shown in Fig. 2(d), when $\Delta\varphi = 0^\circ$, which is the equal amplitude and the same phase, the E_y component distribution is mainly focused on the first quadrant (I) and the second quadrant (II), and the color diagram are similar and symmetrical distribution. This shows that the antenna surface currents are reverse distribution along the y -axis, and the even-mode is the main working mode.

Fig. 2(e) and (f) shows the E_y component distribution (yoz plane) when $\Delta\varphi = 30^\circ$ and $\Delta\varphi = 60^\circ$, respectively. It is

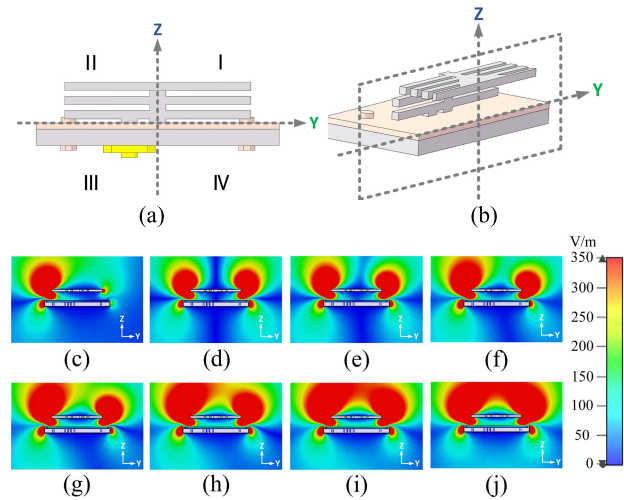


Fig. 2. Simulated E_y component distribution (yoz plane) of the proposed antenna unit: (a) front view, (b) side view, (c) only Port 1 excited, (d) $\Delta\varphi = 0^\circ$, (e) $\Delta\varphi = 30^\circ$, (f) $\Delta\varphi = 60^\circ$, (g) $\Delta\varphi = 90^\circ$, (h) $\Delta\varphi = 120^\circ$, (i) $\Delta\varphi = 150^\circ$, and (j) $\Delta\varphi = 180^\circ$.

obvious that when the phase difference $\Delta\varphi$ is changed of the two feed ports, the E_y component is still distributed in both the first quadrant (I) and the second quadrant (II). It is interesting that the E_y component intensity gradually transfers from the first quadrant (I) to the second quadrant (II). With the phase difference $\Delta\varphi$ increasing from 30° to 60° , the colored diagram is changed to become asymmetrically distributed. In other words, although the even mode is dominant mode, the odd mode is also excited. In fact, this operating mode is hybrid mode.

As the phase difference $\Delta\varphi$ further changes, the phase difference $\Delta\varphi$ increases from 90° , to 120° and then to 150° , and the component distribution of these states is shown in Fig. 2(g)–(i). The E_y component is changed significantly, and it can be seen that the E_y component intensity is not changed obviously in the first quadrant (I), while the E_y component sustained growth in the second quadrant (II). It shows that the odd-mode gradually becomes the dominant mode in hybrid mode, and the influence of the even mode becomes weaker.

The antenna unit operating in the odd mode ($\Delta\varphi = 180^\circ$) is shown in Fig. 2(j), and the odd mode is the main work mode of the proposed antenna unit. We can see that the E_y component covers the first quadrant (I) and the second quadrant (II) equally, and there is strong red color (strong) electric field along the z -axis, which means that the surface currents transfer in the same direction along the y -axis.

By analysis of the E_y components (yoz plane) variation trend, it shows that, as the phase difference $\Delta\varphi$ is changed between the two feed ports, the antenna unit surface current transmission direction and the phase distribution are changed, that is to say, the proposed antenna unit can work in continuous switching operation mode of the even mode, hybrid mode, and odd mode.

2) Radiation Patterns Varying With the Phase Difference $\Delta\varphi$: Fig. 3 shows the radiation patterns that the proposed antenna unit works in the different modes with the different phase differences $\Delta\varphi$.

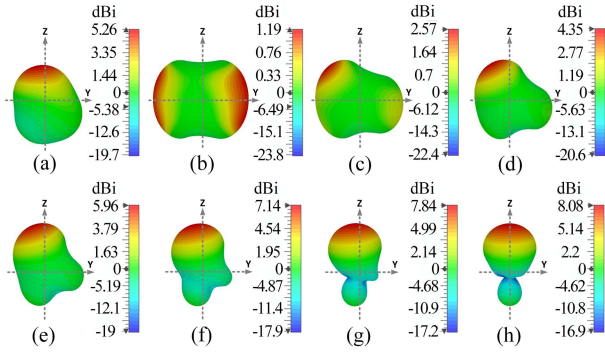


Fig. 3. Simulated radiation patterns (yoz plane) of the proposed antenna unit: (a) only Port 1 excited, (b) $\Delta\varphi = 0^\circ$, (c) $\Delta\varphi = 30^\circ$, (d) $\Delta\varphi = 60^\circ$, (e) $\Delta\varphi = 90^\circ$, (f) $\Delta\varphi = 120^\circ$, (g) $\Delta\varphi = 150^\circ$, and (h) $\Delta\varphi = 180^\circ$.

Only Port 1 is excited as shown in Fig. 3(a), in which the radiation pattern is similar to the endfire lobe, the gain is about 5.3 dBi, and its operation mode is the odd-mode dominant characteristic.

In Fig. 3(b), when $\Delta\varphi = 0^\circ$, the radiation pattern is the broadside radiation characteristic (even mode). The main lobe gain is about 1.2 dBi. The radiation patterns with $\Delta\varphi = 30^\circ$ and 60° are shown in Fig. 3(c) and (d), respectively, which shows the asymmetric distribution characteristic. The reason is that the operation mode of the proposed antenna unit is the hybrid mode, and the gains are about 2.6 and 4.4 dBi. As the phase difference $\Delta\varphi$ increases from 90° to 120° and then to 150° , the patterns are shown in Fig. 3(e)–(g). The main lobe of the radiation patterns is mainly focused on the second quadrant (II), while the main lobe continuously transits from the second quadrant (II) to the first quadrant (I). It means that the proposed antenna unit operates in hybrid mode, and the endfire radiation (odd mode) gradually becomes dominant. The simulated gains are about 6, 7.1, and 7.8 dBi. As shown in Fig. 3(h), when $\Delta\varphi = 180^\circ$, the proposed antenna unit behaves as the endfire characteristic, and its main lobe points to the z -axis. This is the typical odd mode, with the gain of approximately 8.1 dBi.

In summary, the dual-port phased antenna unit based on fishbone structure can perform continuous beam scanning (in the yoz plane) by adjusting the dual-port phase difference $\Delta\varphi$. A new phased antenna unit is provided for the improvement of the wide-angle scanning performance of the phased array. The proposed phased array not only improves the wide-angle scanning performance through array factor functions and optimized array element spacing but also introduces flexible and adjustable element factor, to realize wide-angle beam scanning characteristic of phased array in multidimensional space.

C. Key Parameters' Analysis

The proposed antenna unit is like short “n” based on a fishbone structure, in which the branches (length $l \times$ width p) are uniformly spaced periodic arrangement. As we know, the surface current of each branch shows the odd-mode, even-mode, or hybrid-mode characteristics under excited of different phase differences $\Delta\varphi$. Meanwhile, considering the coupling effects of the branches, which affect the EM characteristics of

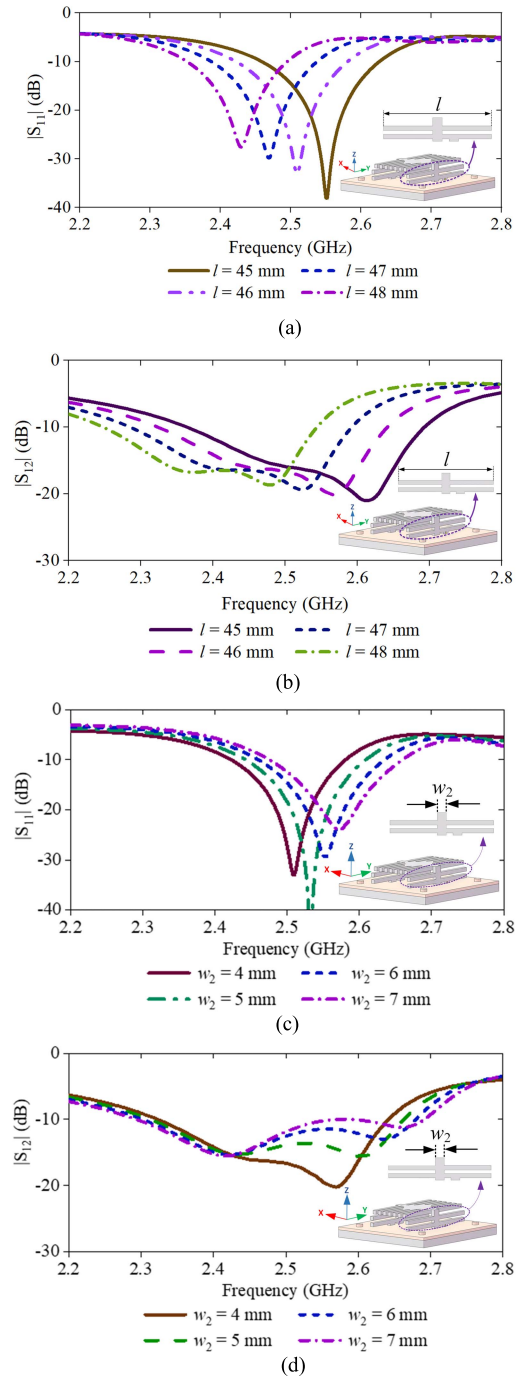


Fig. 4. Key parameters l and w_2 effect on (a) and (c) $|S_{11}|$ and (b) and (d) $|S_{12}|$ of the proposed antenna unit.

the antenna unit, eventually, l and w_2 are the key parameters of the proposed antenna unit, as shown in Fig. 4. Also, their effects on resonant operating frequency and coupling coefficients and so on are further discussed.

1) *Parameter l* : By analysis, the resonant frequency variation trend for the $l = 45, 46, 47,$ and 48 mm is shown in Fig. 4(a).

Obviously, from the S-parameter curves of $l = 45$ mm (the resonant frequency of about 2.55 GHz), $l = 46$ mm (the resonant frequency of about 2.51 GHz), $l = 47$ mm (the resonant frequency of about 2.468 GHz), and $l = 48$ mm (the

TABLE I
OPTIMIZED GEOMETRIC PARAMETERS FOR THE
PROPOSED ANTENNA UNIT

Parameters	s	p	m	n	w_1	w_2
Values / mm	1.5	2	21.3	16	4	4
Parameters	l	d	h	th_1	th_2	th_3
Values / mm	46	27	10	2	1.524	4

resonant frequency of about 2.43 GHz), it can be seen that as l increases from 45 to 48 mm, the resonant frequency shifts to lower frequency and vice versa. This indicates that the branch length l of fishbone structure has a significant effect on the resonant frequency of the antenna unit.

Furthermore, it can be observed from Fig. 4(b) that the coupling coefficients are all less than -13 dB at a center frequency of 2.5 GHz; nevertheless, the coupling coefficients ($|S_{12}|$) migration tends to lower frequency as l increases from 45 to 48 mm. This variation trend characteristic is similar to the resonant frequency change trend.

2) *Parameter w_2* : Fig. 4(c) and (d) shows the variation trends of the reflection coefficient and coupling coefficients being related to the main axis width w_2 in fishbone structure, respectively. In Fig. 4(c), the key parameter w_2 increases from 4 to 7 mm, while the resonant operating frequency shifts from 2.51 to 2.572 GHz. It is obvious that the main axis of the fishbone can not only stabilize the entire antenna unit structure but also serve as a main transmission path for surface currents. When w_2 increases, the resonant frequency of the antenna unit is shifted to higher operating band. Fig. 4(d) shows that the coupling coefficient ($|S_{12}|$) is approximately -20.2 dB ($w_2 = 4$ mm), -14.5 dB ($w_2 = 5$ mm), -11.5 dB ($w_2 = 6$ mm), and -10 dB ($w_2 = 7$ mm) at the center frequency of 2.5 GHz. It is noted that the simulated coupling coefficient ($|S_{12}|$) deteriorates as w_2 increases. The main reason is that the surface current transmission path is widened, which further enhances the coupling effect between the two feed ports.

The above simulation and analysis of the key parameters reveal that the factors affecting the performance of the proposed antenna unit are manifold. Comprehensive assessments of the effect of each parameter on the antenna characteristics have laid the groundwork for the linear array. Finally, the optimal parameters of the proposed antenna unit are shown in Table I.

D. Comparison Between Simulated and Measured Results

1) *Fabricated Prototype of the Proposed Antenna Unit*: Based on the analysis above, evaluation, and Table I, the proposed prototype antenna unit was fabricated and measured in a microwave anechoic chamber. The prototype antenna unit is shown in Fig. 5.

2) *S-Parameters*: The S-parameters of the proposed antenna unit are shown in Fig. 5. It can be seen that the available bandwidth with measured $|S_{11}| < -10$ dB is about 2.42–2.58 GHz (6.4%); meanwhile, the simulated $|S_{11}| < -10$ dB bandwidth is about 2.42–2.58 GHz (6.4%). Note that the measured and simulated results of $|S_{11}|$ agree well. In addition, the measured

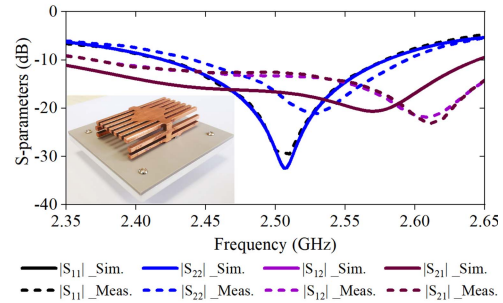


Fig. 5. Simulated and measured S-parameters and the prototype antenna unit.

$|S_{22}| < -10$ dB bandwidth is about 2.44–2.59 GHz (6%), and the simulated $|S_{22}| < -10$ dB bandwidth is approximately 2.42–2.58 GHz (6.4%). Furthermore, the measured $|S_{12}| < -10$ dB is about 2.37–2.68 GHz, and at 2.5 GHz, it is -13.3 dB. The simulated $|S_{12}| < -10$ dB is about 2.33–2.64 GHz, while at 2.5 GHz, it is -16.6 dB. It can be seen that the measured S-parameters trends and available range are close to the simulated results.

It should be noted that the results for simulated $|S_{11}|$ and $|S_{22}|$ overlap and for simulated $|S_{12}|$ and $|S_{21}|$ as well, which is due to structural symmetry and symmetric feeding. However, fabrication errors and the test environment can lead to the inconsistency between the simulated and measured results.

3) *Radiation Patterns*: The simulated and measured radiation patterns of the proposed antenna unit are shown in Fig. 6. It can be seen that, when $\Delta\varphi = 0^\circ$, the radiation patterns of the proposed antenna unit at 2.5 GHz show broadside radiation characteristic, and the simulated results agree well with the measured results. There are two radiation lobes approximately symmetrically distributed in the yo z plane, as shown in Fig. 6(a). Thus, the proposed antenna unit shows the typical broadside radiation characteristics from the even mode. Meanwhile, it can be observed that the phase difference $\Delta\varphi = 0^\circ$, and the main lobe direction $\theta_{me} = -68^\circ$ in the yo z plane. The measured half-power beamwidth (HPBW) is about 77.4° and the simulated HPBW is about 123° .

In particular, there exists a deviation between the measured and simulated results for the HPBW. The experimental results show that the radiation lobe of the proposed antenna unit has small valleys from about 100° to 142° and from 218° to 262° . As mentioned above, the radiation characteristics are very sensitive to the machining accuracy of the antenna metal arms.

As shown in Fig. 6(b), the proposed antenna unit works in hybrid mode ($\Delta\varphi = 30^\circ$). In other words, $\Delta\varphi = 30^\circ$, and the even mode is still the dominant operating mode, while the odd mode is also excited. It is obvious that the main lobe direction is shifted to about $\theta_{me} = -43^\circ$, and the measured HPBW is about 84° . The reasons for the inconstancy of the HPBW results are the same as above and will not be restated. Fig. 6(c)–(e) shows that the proposed antenna unit can achieve wide-angle scanning characteristics, and the main beam lobe (θ_{me}) scanning is from -28° to -18° and then to -5° . The measured HPBW is about 80.8° , 70.7° , and 66° . As discussed above, with the phase difference $\Delta\varphi$ increasing

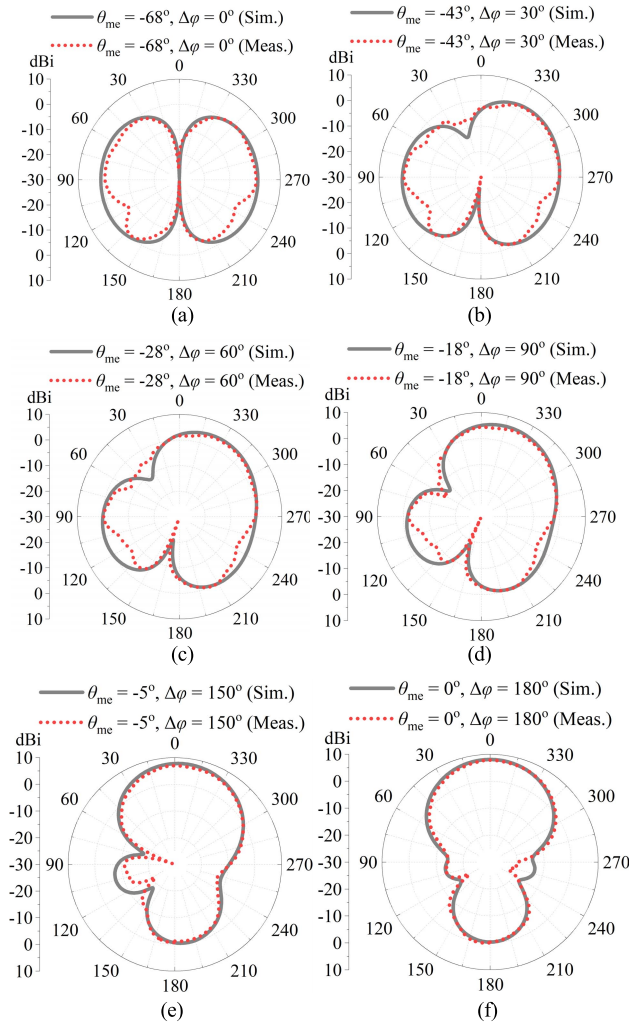


Fig. 6. Comparison between the simulated and the measured radiation patterns (yoz plane) of the proposed antenna unit at 2.5 GHz with different phase differences $\Delta\varphi$. (a) $\Delta\varphi = 0^\circ$ and $\theta_{me} = -68^\circ$. (b) $\Delta\varphi = 30^\circ$ and $\theta_{me} = -43^\circ$. (c) $\Delta\varphi = 60^\circ$ and $\theta_{me} = -28^\circ$. (d) $\Delta\varphi = 90^\circ$ and $\theta_{me} = -18^\circ$. (e) $\Delta\varphi = 150^\circ$ and $\theta_{me} = -5^\circ$. (f) $\Delta\varphi = 180^\circ$ and $\theta_{me} = 0^\circ$.

from 60° and 90° and then to 150° , the proposed antenna unit operates in hybrid mode, that is to say, the broadside radiation (even mode) gradually weakens when the phase difference $\Delta\varphi$ changes from 60° to 150° and the endfire radiation (odd mode) gradually grows. In the meantime, as the odd mode and the even mode continue to shift, the main lobe direction of the proposed antenna unit is changed continuously.

As shown in Fig. 6(f), when the phase difference $\Delta\varphi = 180^\circ$, the antenna works in odd mode with endfire, and the main lobe direction is $\theta_{me} = 0^\circ$. The measured HPBW is about 64° , which is close to the simulated HPBW about 64.2° .

All in all, when the phase difference $\Delta\varphi$ increases from 0° , 30° , 60° , 90° , 150° , to 180° , operation mode switches from the even mode, to hybrid mode, and finally to odd mode.

As a result, the main lobe (in the yoz plane) of the proposed antenna unit prototype shifts from -68° , -43° , -28° , -18° , -5° , to 0° , i.e. the proposed antenna unit exhibits continuous wide-angle beam scanning characteristic, which lays the foundation for the wide-angle beam scanning and multidimensional space scanning of the plane array.

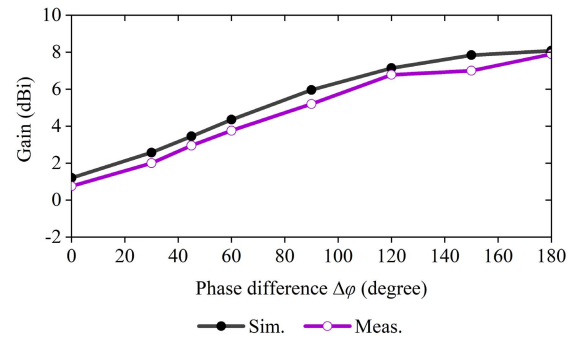


Fig. 7. Simulated and measured gains varying with the phase difference $\Delta\varphi$ at 2.5 GHz.

TABLE II
SCANNING CAPABILITY OF THE ANTENNA ELEMENT
CONTROLLED BY PHASE DIFFERENCE $\Delta\varphi$

$\Delta\varphi$	0°	30°	45°	60°	90°	120°	150°	180°
θ_{me}	-68°	-43°	-35°	-28°	-18°	-11°	-5°	0°
HPBW	77°	84°	85°	81°	71°	69°	66°	64°

4) *Gains*: The realized gain varied with phase difference $\Delta\varphi$ is shown in Fig. 7. As the phase difference $\Delta\varphi$ increases from 0° to 180° , the measured gain increases from 0.75 to 7.9 dBi with the phase difference, which is also according to the variation of the radiation mode of the proposed antenna. Also, the measured results are basically in agreement with the simulated except little difference.

To sum up, through analyzing on the radiation characteristics of the proposed antenna unit, it shows that as the phase difference $\Delta\varphi$ changes, the surface current direction is changed; meanwhile, the odd mode, hybrid mode, and even mode are continuously switched and continuous beam lobe scanning characteristic from -68° to 0° (yoz plane) is further realized. The beam scanning performances of the proposed antenna unit controlled by phase difference $\Delta\varphi$ are shown in Table II.

III. TWO KINDS OF 1-D LINEAR ARRAY WITH SCANNING IN WIDE 2-D CHARACTERISTIC

A. Generalized Principle of Pattern Multiplication

Based on the previous discussion, to improve the wide-angle scanning performance of the directional antenna unit, to expand array wide-angle scanning and the multidimensional space scanning performance are new challenges. The GPPM [41]–[43] was proposed, where the phase difference $\Delta\varphi$ is adjusted between dual-port of the antenna unit to change the transmission direction of the surface currents, meanwhile exciting the different operating modes, such as the odd mode, hybrid mode, and even mode. In other words, the main lobe of the proposed phased antenna unit is no longer limited to the fixed directional pattern, but a flexible and changeable lobe with wide-angle scanning characteristics. Furthermore, the array based on the proposed phased antenna unit can realize beam scanning with the flexible element factor and array factor or the phase difference $\Delta\varphi$ between the dual-port

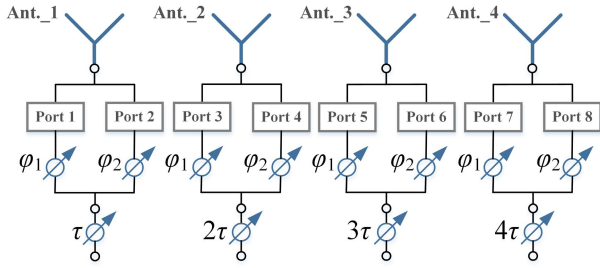


Fig. 8. Configuration of the 1×4 linear array based on the GPPM.

of the antenna unit and the phase difference τ between the adjacent elements.

The array configuration based on the principle is shown in Fig. 8. As an example, four identical dual-port phased antenna units are denoted as Ant._1, Ant._2, Ant._3, and Ant._4, with the feed ports numbered as Ports 1–8.

Therefore, the antenna units have the same initial phase set, which is (φ_1, φ_2) , where the phase difference between Ports 1 and 2 is $\Delta\varphi = \varphi_2 - \varphi_1$, while the phase difference between every two adjacent antenna units is τ .

It can be seen that the GAF of the dual-port antenna unit can also be expressed as

$$f_a(\theta, \Phi, \theta_{ma}, \Phi_{ma}) = f_a(\theta, \Phi, \theta_{ma}(\tau), \Phi_{ma}(\tau)). \quad (1)$$

τ is the phase difference between adjacent antenna units. Meanwhile, the GEF is denoted as

$$f_e(\theta, \Phi, \theta_{me}, \Phi_{me}) = f_e(\theta, \Phi, \theta_{me}(\Delta\varphi), \Phi_{me}(\Delta\varphi)). \quad (2)$$

Thus, the GPPM can be written as

$$\begin{aligned} f(\theta, \Phi, \theta_m, \Phi_m) &= f_a(\theta, \Phi, \theta_{ma}, \Phi_{ma}) \times f_e(\theta, \Phi, \theta_{me}, \Phi_{me}) \\ &= f_a(\theta, \Phi, \theta_{ma}(\tau), \Phi_{ma}(\tau)) \\ &\quad \times f_e(\theta, \Phi, \theta_{me}(\Delta\varphi), \Phi_{me}(\Delta\varphi)). \end{aligned} \quad (3)$$

It is evident that (3) has introduced total of four variables, $\theta_{ma}(\tau)$, $\Phi_{ma}(\tau)$, $\theta_{me}(\Delta\varphi)$, and $\Phi_{me}(\Delta\varphi)$, which vary along the θ -direction and Φ -direction. It means that the degree of freedom of the array in wide-angle beam scanning applications is increased, which is advantageous for improving the performance of the array in wide-angle scanning as well as in 2-D space scanning. It can be seen from this discussion that the proposed dual-port phased antenna unit based on fishbone structure is just a good GEF element, which may achieve wide-angle beam scanning characteristics in 2-D space for the 1×4 1-D linear array, more specifically, in the xoz plane (θ_m), yo z plane (θ_m), and xoy plane (Φ_m) by adjusting the GEF function, the GAF function, and the array layout. The phase states of all ports inside the antenna array are shown in Table III.

In reality, the proposed antenna unit can be extended to 1-D linear array in three arrangements, vertical arrangement (Array#1), oblique 45 arrangement (Array#2), and the horizontal arrangement (Array#3). For Array#3, the y -side length is larger than the x -side length of the antenna unit so that the interval between the adjacent elements is larger and limits the scanning ability of Array#3. Thus, we only discuss Array#1

TABLE III
PHASE OF EACH PORT OF THE ANTENNA UNIT

Number	Port 1	Port 2	Port 3	Port 4
Port Phase / (degree)	φ_1	$\varphi_1 + \Delta\varphi$	$\varphi_1 + \tau$	$\varphi_1 + \tau + \Delta\varphi$
Number	Port 5	Port 6	Port 7	Port 8
Port Phase / (degree)	$\varphi_1 + 2\tau$	$\varphi_1 + \Delta\varphi + 2\tau$	$\varphi_1 + 3\tau$	$\varphi_1 + 3\tau + \Delta\varphi$

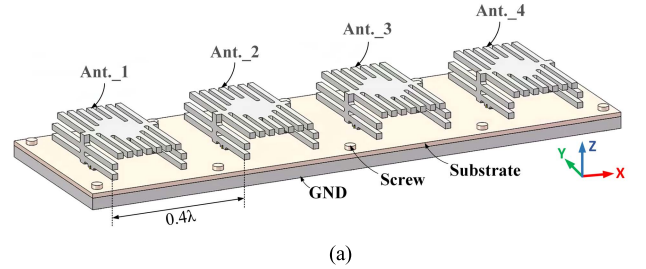


Fig. 9. Configuration of the proposed Array#1: (a) side view, (b) fabricated prototype of the proposed Array#1 and measured the prototype in the microwave anechoic chamber.

and Array#2. To enlarge the scanning angle and suppress grating lobe, the element spacing is usually set to be less than half wavelength [44] or equal to half wavelength.

B. Array#1 (1×4 1-D Linear Array)

The configuration of the proposed Array#1 and the fabricated prototype of the proposed Array#1 are shown in Fig. 9. The proposed Array#1 is linearly arranged along the x -axis, with the array spacing 0.4λ . The phase-shifting network in measurement was composed of a one-to-eight equal-split power divider, eight 8 bit phase shifters, and some phase compensating cable.

1) *S-Parameters of Array#1*: The measured and simulated S-parameters of the proposed Array#1 are shown in Fig. 10(a). The measured $|S_{11}| < -10$ dB band is about 2.43–2.56 GHz, the simulated is 2.38–2.54 GHz, and the center of the measured results moved a little to the lower band. Similarly, the measured available bands of $|S_{22}|$, $|S_{33}|$, $|S_{44}|$, $|S_{55}|$, $|S_{66}|$, $|S_{77}|$, and $|S_{88}|$ are 2.4–2.56, 2.43–2.57, 2.34–2.56, 2.43–2.57, 2.43–2.56, 2.39–2.55, and 2.42–2.5 GHz, respectively. Compared to the simulated reflection coefficient curves of these ports, the measured reflection coefficient curves moved to the lower band a little. Significantly, the simulated S-parameters curves overlap visually.

The coupling coefficients for the proposed Array#1 are shown in Fig. 10(b). It can be seen that the measured $|S_{12}|$,

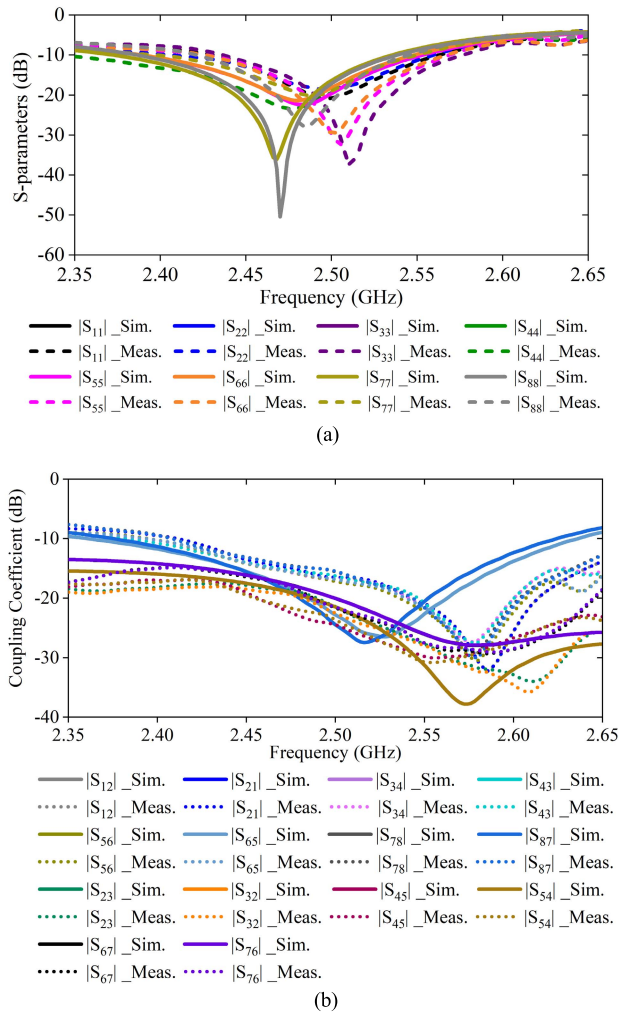


Fig. 10. (a) Simulated and measured S-parameters of the proposed Array#1. (b) Simulated and measured coupling coefficients of the proposed Array#1.

$|S_{21}|$, $|S_{34}|$, $|S_{43}|$, $|S_{56}|$, $|S_{65}|$, $|S_{78}|$, $|S_{87}|$, $|S_{23}|$, $|S_{32}|$, $|S_{45}|$, $|S_{54}|$, $|S_{67}|$, and $|S_{76}|$ are in good agreement, and the overall bands are from about 2.4 to 2.65 GHz with the coupling coefficients being less than -10 dB. Meanwhile, the measured curves are close to the simulated one, besides 0.03 GHz offset to low frequency. In fact, the coupling coefficients are less than -15 dB at the center frequency of 2.5 GHz, whether in simulation or measurement.

2) *Measured and Simulated Beam Scanning Results in 2-D Space for Array#1*: From (3), the proposed dual-port phased antenna unit and the corresponding 1-D linear array combined with the GPPM can realize 2-D space beam scanning [xoz plane (θ_m), yoz plane (θ_m), and xoy plane (Φ_m)] by adjusting the GEF, the GAF, and their matching relationship.

a) *Beam scanning in xoz plane*: For Array#1, the main beam scanning to 2-D space can be realized with varying phase difference ($\Delta\phi$, $\Delta\tau$). The direction of the main beam with different phase differences ($\Delta\phi$, $\Delta\tau$) for Array#1 is shown in Fig. 11 (xoz plane).

As shown in Fig. 11(a) in the xoz plane, when the phase difference ($\Delta\phi$, $\Delta\tau$) = (180° , 0°), the main beam direction is $\theta_m = 0^\circ$. The measured and simulated results match relatively

well, and meanwhile, the measured first sidelobe level is about -11 dB and the measured HPBW is approximately 29.4° , which is close to the simulated results. In Fig. 11(b), the main beam direction is $\theta_m = -30^\circ$ when the phase difference ($\Delta\phi$, $\Delta\tau$) = (90° , 80°). In Fig. 11(c), the main beam direction is $\theta_m = -53^\circ$ when the phase difference ($\Delta\phi$, $\Delta\tau$) = (120° , 170°). In Fig. 11(d), the main beam direction is $\theta_m = -93^\circ$ with the phase difference ($\Delta\phi$, $\Delta\tau$) = (100° , 170°), and $\theta_m = -116^\circ$ with ($\Delta\phi$, $\Delta\tau$) = (150° , 140°) in Fig. 11(e). Apparently, the main beam scanning in the xoz plane is realized by Array#1 with varying ($\Delta\phi$, $\Delta\tau$). With the increase in θ_m , the HPBW is widened too. However, there are few errors in the simulated and measured HPBWs, which are mainly due to errors in the accuracy of the manufacturing process.

b) *Beam scanning in yoz plane*: The measured wide-angle beam scanning performances of the proposed Array#1 in the yoz plane are compared with simulated results, as shown in Fig. 12. It is noteworthy that the beam scanning performance of Array#1 in the yoz plane mainly relies on the even mode. In other words, Array#1 can achieve wide-angle beam scanning characteristic in the yoz plane by adjusting the even mode, hybrid mode, and odd mode of the antenna unit. The operating principle and radiation characteristics of the even mode have been demonstrated in Section II, and thus, to avoid repetition, it is not described in this section.

As shown in Fig. 12(a), when the phase difference ($\Delta\phi$, $\Delta\tau$) = (180° , 0°), the main beam direction is 0° (yoz plane), which is the endfire radiation. The measured HPBW is about 61° , and the measured first sidelobe level is about -13.3 dB.

In Fig. 12(b), when the phase difference ($\Delta\phi$, $\Delta\tau$) = (90° , 0°), the main beam direction is 22° (yoz plane) and the HPBW is about 65.3° . When the phase difference ($\Delta\phi$, $\Delta\tau$) = (40° , 0°), the main beam direction is 41° (yoz plane) in Fig. 12(c), and it can be seen that Array#1 exhibits more obvious even-mode characteristics, i.e., the two beams are progressively similar in shape, while the HPBW covers a larger area, about 133° . As shown in Fig. 12(d) and (e), when the phase difference ($\Delta\phi$, $\Delta\tau$) = (20° , 0°) and ($\Delta\phi$, $\Delta\tau$) = (0° , 0°), the main beam directions are at 51° and 63° , respectively. Meanwhile, the measured HPBWs are about 90° and 93° .

The measured and simulated radiation patterns basically match. Fig. 12(e) shows almost the same symmetrical beam (broadside radiation), and it suggests that the radiation characteristics of the two radiation beams are approximately the same shape, especially the even mode.

c) *Beam scanning in xoy plane*: Next, the measured main beam scanning in the xoy plane is shown in Fig. 13. In Fig. 13(a), the phase difference ($\Delta\phi$, $\Delta\tau$) = (0° , 0°), Array#1 works in the even mode, and meanwhile, the radiation patterns are broadside, i.e., there are a pair of symmetrically distributed beams and the main beam direction is $\Phi_m = 90^\circ$. In Fig. 13(b), the main beam direction is about $\Phi_m = 127^\circ$ with the phase difference ($\Delta\phi$, $\Delta\tau$) = (0° , 90°). Also, the main beam points to $\Phi_m = 143^\circ$ with the phase difference ($\Delta\phi$, $\Delta\tau$) = (0° , 120°) in Fig. 13(c). It can be seen that with the constant change of the phase difference ($\Delta\phi$, $\Delta\tau$), the main beam direction of the proposed Array#1 gradually moves from broadside to endfire in the hybrid operation mode

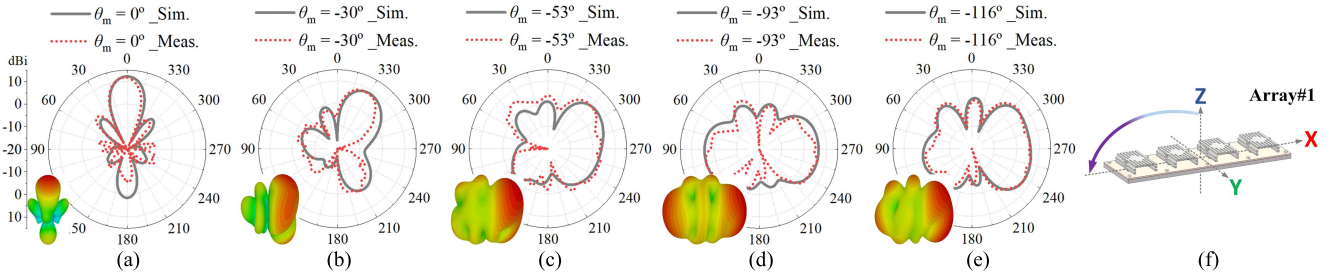


Fig. 11. Radiation patterns (xoz plane) of the proposed Array#1 with phase difference $(\Delta\phi, \Delta\tau)$ change. (a) $\theta_m = 0^\circ$ and $(\Delta\phi, \Delta\tau) = (180^\circ, 0^\circ)$. (b) $\theta_m = -30^\circ$ and $(\Delta\phi, \Delta\tau) = (90^\circ, 80^\circ)$. (c) $\theta_m = -53^\circ$ and $(\Delta\phi, \Delta\tau) = (120^\circ, 170^\circ)$. (d) $\theta_m = -93^\circ$ and $(\Delta\phi, \Delta\tau) = (100^\circ, 170^\circ)$. (e) $\theta_m = -116^\circ$ and $(\Delta\phi, \Delta\tau) = (150^\circ, 140^\circ)$. (f) Side view of Array#1.

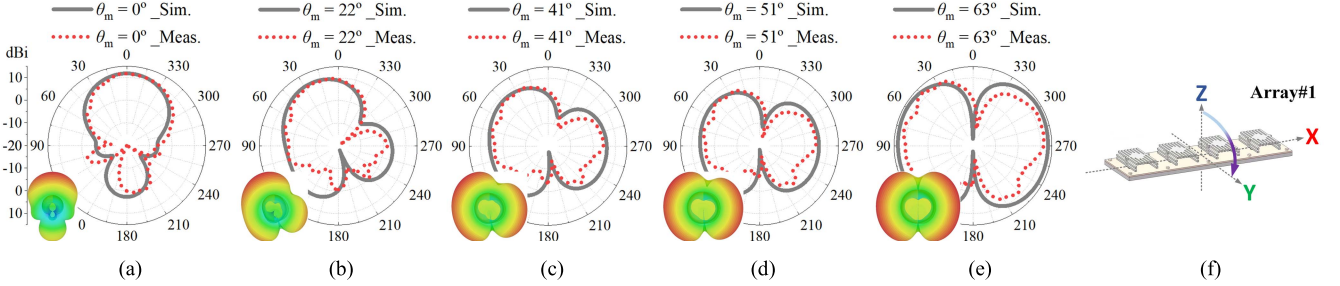


Fig. 12. Radiation patterns (yoz plane) of the proposed Array#1 with phase difference $(\Delta\phi, \Delta\tau)$ change. (a) $\theta_m = 0^\circ$ and $(\Delta\phi, \Delta\tau) = (180^\circ, 0^\circ)$. (b) $\theta_m = 22^\circ$ and $(\Delta\phi, \Delta\tau) = (90^\circ, 0^\circ)$. (c) $\theta_m = 41^\circ$ and $(\Delta\phi, \Delta\tau) = (40^\circ, 0^\circ)$. (d) $\theta_m = 51^\circ$ and $(\Delta\phi, \Delta\tau) = (20^\circ, 0^\circ)$. (e) $\theta_m = 63^\circ$ and $(\Delta\phi, \Delta\tau) = (0^\circ, 0^\circ)$. (f) Side view of Array#1.

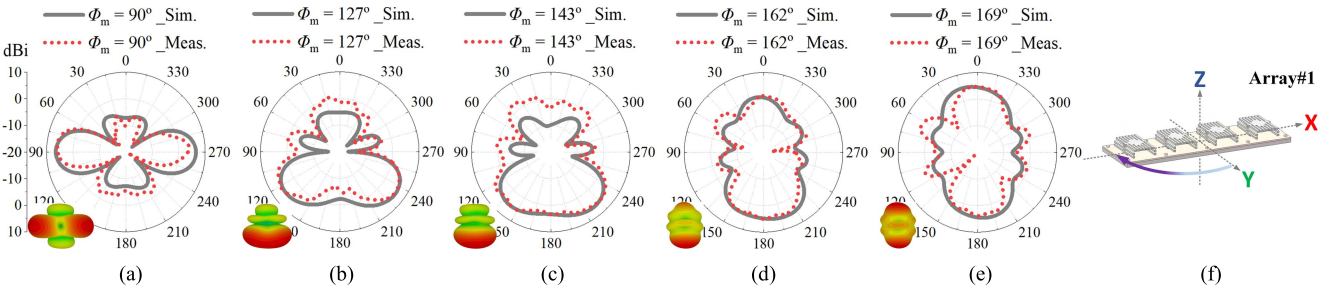


Fig. 13. Radiation patterns (xoy plane) of the proposed Array#1 with phase difference $(\Delta\phi, \Delta\tau)$ change. (a) $\Phi_m = 90^\circ$ and $(\Delta\phi, \Delta\tau) = (0^\circ, 0^\circ)$. (b) $\Phi_m = 127^\circ$ and $(\Delta\phi, \Delta\tau) = (0^\circ, 90^\circ)$. (c) $\Phi_m = 143^\circ$ and $(\Delta\phi, \Delta\tau) = (0^\circ, 120^\circ)$. (d) $\Phi_m = 162^\circ$ and $(\Delta\phi, \Delta\tau) = (0^\circ, 160^\circ)$. (e) $\Phi_m = 169^\circ$ and $(\Delta\phi, \Delta\tau) = (0^\circ, 180^\circ)$. (f) Side view of Array#1.

in the xoy plane. In Fig. 13(d), the main beam direction is about $\Phi_m = 162^\circ$ with the phase difference $(\Delta\phi, \Delta\tau) = (0^\circ, 160^\circ)$, and in Fig. 13(e), the main beam points to $\Phi_m = 169^\circ$ with the phase difference $(\Delta\phi, \Delta\tau) = (0^\circ, 180^\circ)$. It was clear that, with phase difference $(\Delta\phi, \Delta\tau)$ changing, the main beam performs scanning characteristic in the xoy plane. Also, the proposed Array#1 radiates from even mode to hybrid mode and then odd mode or broadside radiation to mixed radiation and to endfire pattern finally.

In conclusion, with phase difference $(\Delta\phi, \Delta\tau)$ changing, Array#1 can perform wide-angle scanning in the 2-D space, 0° to -116° in the xoz plane, 0° – 63° in the yoz plane, and 90° – 169° in the xoy plane.

C. Array#2 (1×4 1-D Linear 45° Array)

In order to reduce the coupling effects between antenna units and improve beam scanning performance of array in 2-D space, the proposed antenna unit is rotated 45° around the z -axis, and four antenna units are extended along the x -axis to construct Array#2, as shown in Fig. 14.

1) *S-Parameters of Array#2*: The measured and simulated S-parameters of the proposed Array#2 are shown in Fig. 15(a). The measured bandwidth is about 2.35–2.54 GHz to $|S_{11}| < -10$ dB, 2.46–2.57 GHz to $|S_{22}| < -10$ dB, 2.44–2.57 GHz to $|S_{33}| < -10$ dB, 2.34–2.55 GHz to $|S_{44}| < -10$ dB, 2.2–2.57 GHz to $|S_{55}| < -10$ dB, 2.44–2.58 GHz to $|S_{66}| < -10$ dB, 2.35–2.54 GHz to $|S_{77}| < -10$ dB, and 2.44–2.57 GHz to $|S_{88}| < -10$ dB. Compared to the simulated curves, all the measured curves shift a little to lower band, but the S-parameters at the center frequency 2.5 GHz are all less than -14 dB.

The coupling coefficients between the adjacent ports for the proposed Array#2 are shown in Fig. 15(b). It can be seen that the measured available band with $|S_{12}|$, $|S_{21}|$, $|S_{56}|$, $|S_{65}|$, $|S_{78}|$, $|S_{87}|$, $|S_{23}|$, $|S_{32}|$, $|S_{45}|$, $|S_{54}|$, $|S_{67}|$, and $|S_{76}|$ less than -10 dB ranges from about 2.35 to 2.6 GHz. Also, the measured and simulated coupling coefficients are less than -11 dB at the center frequency of 2.5 GHz.

2) *Measured and Simulated Beam Scanning Results in 2-D Space for Array#2*: From (3), the proposed dual-port phased

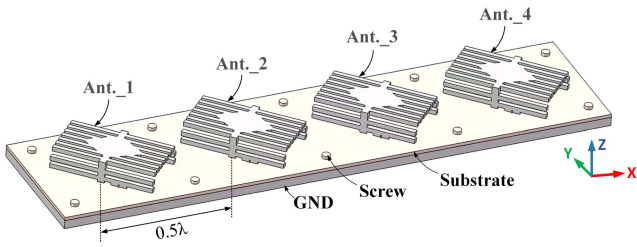


Fig. 14. Configuration of the proposed Array#2.

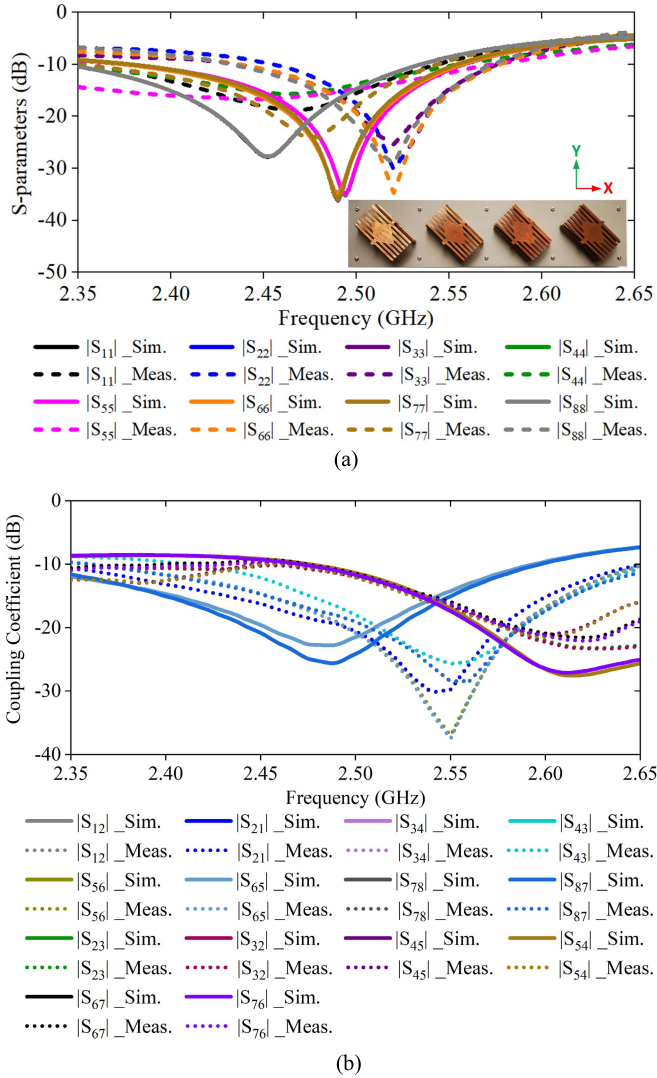


Fig. 15. (a) Simulated and measured S-parameters of the proposed Array#2 and fabricated prototype of the proposed Array#2. (b) Simulated and measured coupling coefficients of the proposed Array#2.

antenna unit and the corresponding 1-D linear Array#2 combined with the GPPM can realize 2-D space beam scanning [xoz plane (θ_m), yoz plane (θ_m), and xoy plane (Φ_m)] by adjusting the GEF, the GAF, and their matching relationship.

a) Beam scanning in xoz plane: For Array#2, the main beam scanning in the xoz plane can be realized with varying phase difference ($\Delta\phi$, $\Delta\tau$).

The beam scanning in the xoz plane with different phase differences ($\Delta\phi$, $\Delta\tau$) for Array#2 is shown in Fig. 16.

The phase difference ($\Delta\phi$, $\Delta\tau$) = (180°, 0°), the proposed Array#2 operates in the odd mode, and the endfire beam is achieved. The measured HPBW is about 22°.

In Fig. 16(b), the measured main beam direction is $\theta_m = -30^\circ$, and the HPBW is about 29° with phase difference ($\Delta\phi$, $\Delta\tau$) = (120°, 100°). Here, the proposed Array#2 operates in hybrid mode, with the odd mode still working as the dominant operation mode. Significantly, Fig. 16(b) shows that when θ_m is around -148° , there is a deviation between measured and simulated results, which is mainly due to machining errors and the uncertain effects of the measurement environment.

As shown in Fig. 16(c), when the phase difference ($\Delta\phi$, $\Delta\tau$) = (100°, 125°), the measured main beam direction is $\theta_m = -40^\circ$ in the xoz plane, the measured first sidelobe level is about -11 dB, and the HPBW is about 31.1°. There is also a deviation of the sidelobe direction around -140° between the measured and simulated results, due to the same reasons for Fig. 16(b). Fig. 16(d) shows that the measured main beam direction $\theta_m = -50^\circ$ and the phase difference ($\Delta\phi$, $\Delta\tau$) = (60°, 145°); meanwhile, the measured first sidelobe level is about -11.8 dB, the measured first sidelobe level is about -11.3 dB, and the HPBW is about 30.4°. The measured and simulated curves are in good agreement. In Fig. 16(e), the measured main beam direction is -60° for Array#2, while the phase difference ($\Delta\phi$, $\Delta\tau$) = (60°, 180°). Furthermore, the measured HPBW is about 38.2° and the measured first sidelobe level is about -5.2 dB.

b) Beam scanning in yoz plane: For Array#2, the main beam scanning in the yoz plane can be realized with varying phase difference ($\Delta\phi$, $\Delta\tau$).

The main beam scanning characteristics of the proposed Array#2 in the yoz plane are discussed in the following. The main beam scanning characteristics in the yoz plane can be achieved, by adjusting the GEF. Fig. 17(a) shows that the measured main beam direction is $\theta_m = 0^\circ$ with the phase difference ($\Delta\phi$, $\Delta\tau$) = (180°, 0°). In addition, the measured HPBW is about 66°. It can be observed that the proposed Array#2 shows the endfire (odd mode), with a good symmetry characteristic of its radiation patterns. In Fig. 17(b)–(d), the proposed Array#2 operates in hybrid mode, which results from the linear superposition of the odd mode and even mode, meanwhile, with phase differences ($\Delta\phi$, $\Delta\tau$) = (80°, 0°), ($\Delta\phi$, $\Delta\tau$) = (50°, 0°), and ($\Delta\phi$, $\Delta\tau$) = (30°, 0°). By observing its radiation patterns, it can be seen that the measured main beam directions of the proposed Array#2 are $\theta_m = 29^\circ$, $\theta_m = 41^\circ$, and $\theta_m = 50^\circ$. Meanwhile, the HPBWs are about 89.3°, 84°, and 80°.

Finally, as shown in Fig. 17(e), the proposed Array#2 operates in the even mode with the main beam direction $\theta_m = 65^\circ$ and ($\Delta\phi$, $\Delta\tau$) = (0°, 0°). Meanwhile, the HPBW is about 74°. In fact, as shown in Fig. 17(d) and (e), when the main beam direction $\theta_m = 50^\circ$ and $\theta_m = 65^\circ$, there are some errors between the simulated and measured HPBWs, that is to say, the machining accuracy has certain effect on the measured results.

c) Beam scanning in xoy plane: For Array#2, the main beam scanning in the xoy plane can be realized with varying phase difference ($\Delta\phi$, $\Delta\tau$).

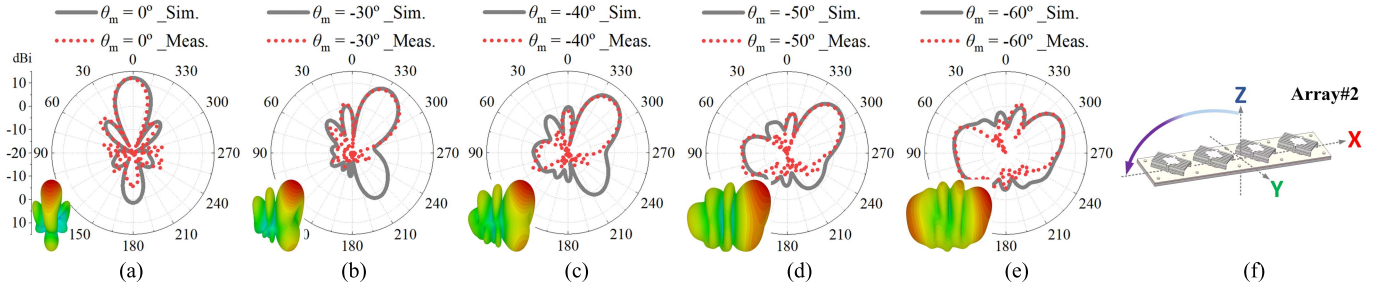


Fig. 16. Radiation patterns (xoz plane) of the proposed Array#1 with phase difference $(\Delta\phi, \Delta\tau)$ change. (a) $\theta_m = 0^\circ$ and $(\Delta\phi, \Delta\tau) = (180^\circ, 0^\circ)$. (b) $\theta_m = -30^\circ$ and $(\Delta\phi, \Delta\tau) = (120^\circ, 100^\circ)$. (c) $\theta_m = -40^\circ$ and $(\Delta\phi, \Delta\tau) = (100^\circ, 125^\circ)$. (d) $\theta_m = -50^\circ$ and $(\Delta\phi, \Delta\tau) = (60^\circ, 145^\circ)$. (e) $\theta_m = -60^\circ$ and $(\Delta\phi, \Delta\tau) = (60^\circ, 180^\circ)$. (f) Side view of Array#2.

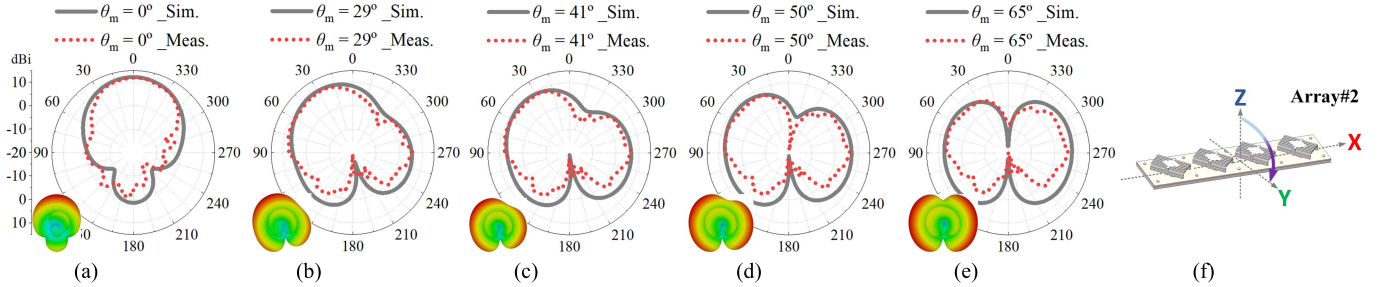


Fig. 17. Radiation patterns (yoz plane) of the proposed Array#2 with phase difference $(\Delta\phi, \Delta\tau)$ change. (a) $\theta_m = 0^\circ$ and $(\Delta\phi, \Delta\tau) = (180^\circ, 0^\circ)$. (b) $\theta_m = 29^\circ$ and $(\Delta\phi, \Delta\tau) = (80^\circ, 0^\circ)$. (c) $\theta_m = 41^\circ$ and $(\Delta\phi, \Delta\tau) = (50^\circ, 0^\circ)$. (d) $\theta_m = 50^\circ$ and $(\Delta\phi, \Delta\tau) = (30^\circ, 0^\circ)$. (e) $\theta_m = 65^\circ$ and $(\Delta\phi, \Delta\tau) = (0^\circ, 0^\circ)$. (f) Side view of Array#2.

TABLE IV
COMPARISON WITH OTHER REPORTED ARRAY

Ref.	Band width (GHz)	Dimensionality of Scanning	Profile	Main Beam Scanning Rang	HPBW		
[8]	3.2 ~ 3.8	1-D, (1 × 9 array)	0.2λ	±90° (H-plane); ±75° (E-plane)	—		
[9]	7.35 ~ 7.6	1-D, (1 × 16 array)	—	66°	—		
[10]	8 ~ 9.5	1-D, (1 × 10 array)	—	±70° (xoz -plane)	—		
[18]	3.2 ~ 3.8	1-D, (1 × 8 array)	—	-89° ~ 90° (E-plane)	-105° ~ 105°		
[43]	4.5 ~ 6	2-D, (1 × 4 array)	0.7λ	Array#2, θ (0° ~ 73°), Φ (0° ~ 50°)	0° < Φ < 140° (Array#2) 0° < θ < 90° (Array#2)		
				Array#3, θ (0° ~ 90°), Φ (0° ~ 40°)	0° < Φ < 180° (Array#3) 0° < θ < 90° (Array#3)		
This work	2.4 ~ 2.6	2-D, (1 × 4 array)	0.08λ	Array#1	xoz -plane	$\theta_m, \pm 116^\circ$	$29.4^\circ < \theta_m < 105^\circ$
					yoz -plane	$\theta_m, \pm 63^\circ$	$59^\circ < \theta_m < 133^\circ$
				xoy -plane	$\Phi_m, \pm 79^\circ$	$32^\circ < \Phi_m < 123^\circ$	
				Array#2	xoz -plane	$\theta_m, \pm 60^\circ$	$22^\circ < \theta_m < 38.2^\circ$
					yoz -plane	$\theta_m, \pm 65^\circ$	$66^\circ < \theta_m < 90^\circ$
xoy -plane	$\Phi_m, \pm 62^\circ$	$27^\circ < \Phi_m < 267^\circ$					

Next, the beam scanning characteristics of Array#2 in the xoy plane are shown in Fig. 18. In Fig. 18(a), Array#2 operates in even mode when $(\Delta\phi, \Delta\tau) = (0^\circ, 0^\circ)$ with main beam direction pointing to $\Phi_m = 90^\circ$ in the xoy plane, meanwhile showing broadside radiation characteristic. It is clearly seen from Fig. 18(b)–(d) that, under the hybrid mode, the proposed Array#2 exhibits double-lobe characteristics in the xoy plane. When the phase differences $(\Delta\phi, \Delta\tau)$ are $(0^\circ, 60^\circ)$, $(0^\circ, 90^\circ)$, and $(0^\circ, 120^\circ)$, the main beam directions are $\Phi_m = 110^\circ$, 120° , and 129° , respectively. Meanwhile, the HPBW is about 30° , 31° , and 31° . Furthermore, the first sidelobe level is about -9.7 , -9.7 , and -9.3 dB. In Fig. 18(e), $(\Delta\phi, \Delta\tau) = (0^\circ, 170^\circ)$ with main beam

direction points to $\Phi_m = 152^\circ$, and it is close to endfire radiation.

To sum up, the proposed antenna unit has a positive effect for improving the 2-D space beam scanning performance (in xoz plane, yoz plane, and xoy plane) when it is rotated 45° along the z -axis.

The proposed two kinds of the 1-D antenna array to 2-D beam scanning are compared with the reported wide-angle scanning array in Table IV. It is noted that the presented 1-D antenna array in this article can realize 2-D beam scanning with profile 0.08λ , which is much smaller than the reported array in [43]. Thus, our array is very suitable for conformal installation of high-speed platform.

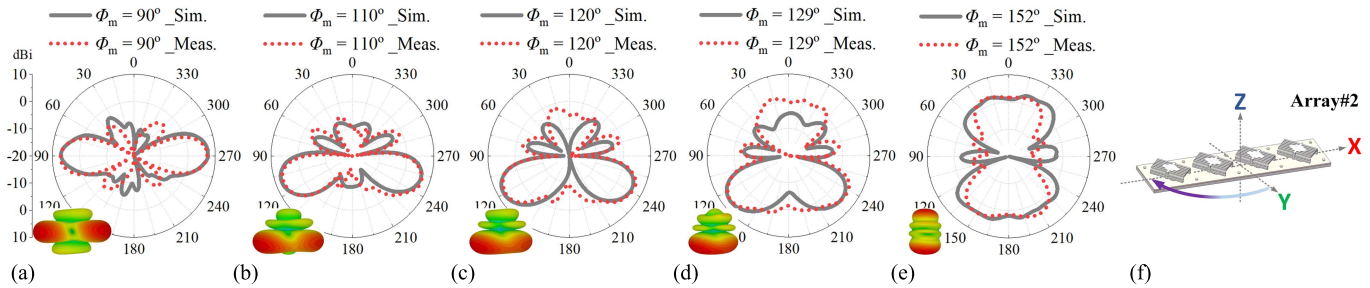


Fig. 18. Radiation patterns (xoy plane) of the proposed Array#2 with phase difference ($\Delta\phi$, $\Delta\tau$) change. (a) $\Phi_m = 90^\circ$ and $(\Delta\phi, \Delta\tau) = (0^\circ, 0^\circ)$. (b) $\Phi_m = 110^\circ$ and $(\Delta\phi, \Delta\tau) = (0^\circ, 60^\circ)$. (c) $\Phi_m = 120^\circ$ and $(\Delta\phi, \Delta\tau) = (0^\circ, 90^\circ)$. (d) $\Phi_m = 129^\circ$ and $(\Delta\phi, \Delta\tau) = (0^\circ, 120^\circ)$. (e) $\Phi_m = 152^\circ$ and $(\Delta\phi, \Delta\tau) = (0^\circ, 170^\circ)$. (f) Side view of Array#2.

IV. CONCLUSION

This article presents a novel low-profile dual-port phased antenna unit based on a fishbone structure. Analysis shows that by adjusting the phase difference $\Delta\phi$ between the dual-port of the antenna, the proposed antenna unit can switch among the odd mode, even mode, and hybrid operation mode. Also, the hybrid mode is the linear superposition of the odd mode and even mode. Finally, the proposed antenna unit achieves continuous beam scanning characteristics from broadside radiation lobe to endfire radiation lobe.

Then, two kinds of the 1×4 1-D linear array (Array#1 and Array#2) are constructed by the 1-D extension of the proposed phased antenna unit. Also, Array#1 and Array#2 prototypes are fabricated based on the proposed antenna unit applying the GPPM. Furthermore, by analyzing the GEF, the GAF, and the arrangement method of the array, it is found that both 1-D arrays (Array#1 and Array#2) can realize wide-angle beam scanning in 2-D space. More specifically, Array#1 achieves -116° to 0° wide-angle scanning along the θ -direction (xoz plane) with gains of about 6.9–11.7 dBi and HPBW of about 29.4° – 105° , 0° – 63° wide-angle scanning along the θ -direction (yoz plane) with gains of about 6.7–11.7 dBi and HPBW of about 59° – 133° , and 90° – 169° wide-angle scanning along the Φ -direction (xoy plane) with gains of about 4.4–6.2 dBi and HPBW of about 32° – 123° . Meanwhile, the proposed Array#2 obtains -60° to 0° beam scanning along the θ -direction (xoz plane) with gains of about 7–12 dBi and HPBW of about 22° – 38.2° , 0° – 65° wide-angle scanning along the θ -direction (yoz plane) with gains of about 7.6–11.9 dBi and HPBW of about 66° – 90° , and 90° – 152° wide-angle scanning along the Φ -direction (xoy plane) with gains of about 4–7.3 dBi and HPBW of about 27° – 267° .

The proposed phased antenna unit and its 1-D linear array (Array#1 and Array#2) based on fishbone structure combined with the GPPM show influential significance for improving the wide-angle beam scanning performance and scanning dimension space of the 1-D linear array. Meanwhile, it has a positive effect on improving future wireless communication systems and radar systems.

ACKNOWLEDGMENT

The authors would like to thank Guolin Tong, Laboratory of Antenna and Scattering, Shanghai Jiao Tong University, Shanghai, China, for his support and assistance in experiment.

REFERENCES

- [1] W. Hong *et al.*, "Multibeam antenna technologies for 5G wireless communications," *IEEE Trans. Antennas Propag.*, vol. 65, no. 12, pp. 6231–6249, Dec. 2017.
- [2] M. Khalily, R. Tafazolli, P. Xiao, and A. A. Kishk, "Broadband mm-wave Microstrip array antenna with improved radiation characteristics for different 5G applications," *IEEE Trans. Antennas Propag.*, vol. 66, no. 9, pp. 4641–4647, Sep. 2018.
- [3] I. Syrytsin, S. Zhang, G. F. Pedersen, and A. S. Morris, "User-shadowing suppression for 5G mm-wave mobile terminal antennas," *IEEE Trans. Antennas Propag.*, vol. 67, no. 6, pp. 4162–4172, Jun. 2019.
- [4] S.-M. Moon, S. Yun, I.-B. Yom, and H. L. Lee, "Phased array shaped-beam satellite antenna with boosted-beam control," *IEEE Trans. Antennas Propag.*, vol. 67, no. 12, pp. 7633–7636, Dec. 2019.
- [5] H. Al-Saedi *et al.*, "A low-cost Ka-band circularly polarized passive phased-array antenna for mobile satellite applications," *IEEE Trans. Antennas Propag.*, vol. 67, no. 1, pp. 221–231, Jan. 2019.
- [6] X. Ding, B.-Z. Wang, and G.-Q. He, "Research on a millimeter-wave phased array with wide-angle scanning performance," *IEEE Trans. Antennas Propag.*, vol. 61, no. 10, pp. 5319–5324, Oct. 2013.
- [7] X. Ding, Y.-F. Cheng, W. Shao, and B.-Z. Wang, "A planar wide-angle scanning phased array with X-, Ku-, and K-band RCS reduction," *IEEE Trans. Antennas Propag.*, vol. 68, no. 5, pp. 4103–4108, May 2020.
- [8] G. W. Yang, J. Y. Li, D. J. Wei, and R. Xu, "Study on wide-angle scanning linear phased array antenna," *IEEE Trans. Antennas Propag.*, vol. 66, no. 1, pp. 450–455, Jan. 2018.
- [9] R.-L. Xia, S.-W. Qu, P.-F. Li, D.-Q. Yang, S. Yang, and Z.-P. Nie, "Wide-angle scanning phased array using an efficient decoupling network," *IEEE Trans. Antennas Propag.*, vol. 63, no. 11, pp. 5161–5165, Nov. 2015.
- [10] F.-L. Jin, X. Ding, Y.-F. Cheng, B.-Z. Wang, and W. Shao, "A wideband phased array with broad scanning range and wide-angle impedance matching," *IEEE Trans. Antennas Propag.*, vol. 68, no. 8, pp. 6022–6031, Aug. 2020.
- [11] Y. Q. Wen, B. Z. Wang, and X. Ding, "A wide-angle scanning and low sidelobe level microstrip phased array based on genetic algorithm optimization," *IEEE Trans. Antennas Propag.*, vol. 64, no. 2, pp. 805–810, Feb. 2016.
- [12] B. A. Arand, A. Bazrkar, and A. Zahedi, "Design of a phased array in triangular grid with an efficient matching network and reduced mutual coupling for wide-angle scanning," *IEEE Trans. Antennas Propag.*, vol. 65, no. 6, pp. 2983–2991, Jun. 2017.
- [13] Y.-Q. Wen, S. Gao, B.-Z. Wang, and Q. Luo, "Dual-polarized and wide-angle scanning microstrip phased array," *IEEE Trans. Antennas Propag.*, vol. 66, no. 7, pp. 3775–3780, Jul. 2018.
- [14] Z. Li *et al.*, "Investigation of leaky-wave antenna with stable wide beam-scanning characteristic," *IEEE Trans. Antennas Propag.*, vol. 70, no. 1, pp. 240–249, Jan. 2022.
- [15] Y.-F. Cheng, X. Ding, W. Shao, M.-X. Yu, and B.-Z. Wang, "2-D planar wide-angle scanning-phased array based on wide-beam elements," *IEEE Antennas Wireless Propag. Lett.*, vol. 16, pp. 876–879, 2017.
- [16] G. Yang, Q. Chen, J. Li, S. Zhou, and Z. Xing, "Improving wide-angle scanning performance of phased array antenna by dielectric sheet," *IEEE Access*, vol. 7, pp. 71897–71906, 2019.
- [17] R. Wang, B.-Z. Wang, C. Hu, and X. Ding, "Wide-angle scanning planar array with quasi-hemispherical-pattern elements," *Sci. Rep.*, vol. 7, no. 1, p. 2729, Jun. 2017.

- [18] R. Wang, B.-Z. Wang, X. Ding, and X.-S. Yang, "Planar phased array with wide-angle scanning performance based on image theory," *IEEE Trans. Antennas Propag.*, vol. 63, no. 9, pp. 3908–3917, Sep. 2015.
- [19] M. Shirazi, T. Li, J. Huang, and X. Gong, "A reconfigurable dual-polarization slot-ring antenna element with wide bandwidth for array applications," *IEEE Trans. Antennas Propag.*, vol. 66, no. 11, pp. 5943–5954, Nov. 2018.
- [20] C. W. Jung, M.-J. Lee, G. P. Li, and F. De Flaviis, "Reconfigurable scan-beam single-arm spiral antenna integrated with RF-MEMS switches," *IEEE Trans. Antennas Propag.*, vol. 54, no. 2, pp. 455–463, Feb. 2006.
- [21] T. Debogovic and J. Perruisseau-Carrier, "Array-fed partially reflective surface antenna with independent scanning and beamwidth dynamic control," *IEEE Trans. Antennas Propag.*, vol. 62, no. 1, pp. 446–449, Jan. 2014.
- [22] S. Fofana, B. Fuchs, S. Avrillon, F. Colombel, L. Leze, and S. Palud, "Reconfigurable antenna array with reduced power consumption—Synthesis methods and experimental validations in S-band," *IEEE Trans. Antennas Propag.*, vol. 69, no. 4, pp. 2023–2030, Apr. 2021.
- [23] Y. Y. Bai, S. Xiao, M. C. Tang, Z. F. Ding, and B. Z. Wang, "Wide-angle scanning phased array with pattern reconfigurable elements," *IEEE Trans. Antennas Propag.*, vol. 59, no. 11, pp. 4071–4076, Nov. 2011.
- [24] D. Zheng, Y.-L. Lyu, and K. Wu, "Transversely slotted SIW leaky-wave antenna featuring rapid beam-scanning for millimeter-wave applications," *IEEE Trans. Antennas Propag.*, vol. 68, no. 6, pp. 4172–4185, Jun. 2020.
- [25] L. Jidi, X. Cao, J. Gao, T. Li, H. Yang, and S. Li, "Ultrawide-angle and high-scanning-rate leaky wave antenna based on spoof surface plasmon polaritons," *IEEE Trans. Antennas Propag.*, vol. 70, no. 3, pp. 2312–2317, Mar. 2022, doi: [10.1109/TAP.2021.3111182](https://doi.org/10.1109/TAP.2021.3111182).
- [26] D. K. Karmokar, Y. J. Guo, S.-L. Chen, and T. S. Bird, "Composite right/left-handed leaky-wave antennas for wide-angle beam scanning with flexibly chosen frequency range," *IEEE Trans. Antennas Propag.*, vol. 68, no. 1, pp. 100–110, Jan. 2020.
- [27] H.-W. Yu, Y.-C. Jiao, C. Zhang, and Z.-B. Weng, "Dual-linearly polarized leaky-wave patch array with low cross-polarization levels using symmetrical spoof surface plasmon polariton lines," *IEEE Trans. Antennas Propag.*, vol. 69, no. 3, pp. 1781–1786, Mar. 2021.
- [28] X. Zhang, L. Sun, Y. Li, and Z. Zhang, "A grooved half-mode waveguide leaky-wave antenna for vertically-polarized endfire radiation," *IEEE Trans. Antennas Propag.*, vol. 69, no. 12, pp. 8229–8236, Dec. 2021.
- [29] A. E. Olk, M. Liu, and D. A. Powell, "Printed tapered leaky-wave antennas for W-band frequencies," *IEEE Trans. Antennas Propag.*, vol. 70, no. 2, pp. 900–910, Feb. 2022.
- [30] Q. L. Zhang, B. J. Chen, K. F. Chan, and C. H. Chan, "High-gain millimeter-wave antennas based on spoof surface plasmon polaritons," *IEEE Trans. Antennas Propag.*, vol. 68, no. 6, pp. 4320–4331, Jun. 2020.
- [31] G. Zhang, Q. Zhang, Y. Chen, and R. D. Murch, "High-scanning-rate and wide-angle leaky-wave antennas based on glide-symmetry Goubau line," *IEEE Trans. Antennas Propag.*, vol. 68, no. 4, pp. 2531–2540, Apr. 2020.
- [32] Y. R. Ding and Y. J. Cheng, "A tri-band shared-aperture antenna for (2.4, 5.2) GHz Wi-Fi application with MIMO function and 60 GHz wigi application with beam-scanning function," *IEEE Trans. Antennas Propag.*, vol. 68, no. 3, pp. 1973–1981, Mar. 2020.
- [33] X. Du, J. Ren, H. Li, C. Zhang, Y. Liu, and Y. Yin, "Design of a leaky-wave antenna featuring beam scanning from backfire utilizing odd-mode spoof surface plasmon polaritons," *IEEE Trans. Antennas Propag.*, vol. 69, no. 10, pp. 6971–6976, Oct. 2021.
- [34] K. Zhuang *et al.*, "Pattern reconfigurable antenna applying spoof surface plasmon polaritons for wide angle beam steering," *IEEE Access*, vol. 7, pp. 15444–15451, 2019.
- [35] X. Du, H. Li, and Y. Yin, "Wideband fish-bone antenna utilizing odd-mode spoof surface plasmon polaritons for endfire radiation," *IEEE Trans. Antennas Propag.*, vol. 67, no. 7, pp. 4848–4853, Jul. 2019.
- [36] Y. Han *et al.*, "Shared-aperture antennas based on even- and odd-mode spoof surface plasmon polaritons," *IEEE Trans. Antennas Propag.*, vol. 68, no. 4, pp. 3254–3258, Apr. 2020.
- [37] M. Du, K. Chen, J. Zhao, and Y. Feng, "Differential signal propagation in spoof plasmonic structure and its application in microwave filtering balun," *IEEE Access*, vol. 8, pp. 109009–109014, 2020.
- [38] L. Jidi, X. Cao, J. Gao, H. Yang, S. Li, and T. Li, "An ultra-thin and compact band-pass filter based on spoof surface plasmon polaritons," *IEEE Access*, vol. 8, pp. 171416–171422, 2020.
- [39] J. Wang *et al.*, "Metantenna: When metasurface meets antenna again," *IEEE Trans. Antennas Propag.*, vol. 68, no. 3, pp. 1332–1347, Mar. 2020.
- [40] I. Kim and Y. Rahmat-Samii, "RF MEMS switchable slot patch antenna integrated with bias network," *IEEE Trans. Antennas Propag.*, vol. 59, no. 12, pp. 4811–4815, Dec. 2011.
- [41] E. Liu *et al.*, "Multi-mode phase slots antenna with dual ports," in *Proc. IEEE Int. Symp. Antennas Propag. North Amer. Radio Sci. Meeting*, Jul. 2020, pp. 691–692.
- [42] E. Liu *et al.*, "Generalized principle of pattern multiplication based on the phase antenna element," in *Proc. IEEE Int. Symp. Antennas Propag. North Amer. Radio Sci. Meeting*, Jul. 2020, pp. 353–354.
- [43] J. Zhang *et al.*, "Dual-port phase antenna and its application in 1-D arrays to 2-D scanning," *IEEE Trans. Antennas Propag.*, vol. 69, no. 11, pp. 7508–7520, Nov. 2021.
- [44] H. Yang, X. Cao, J. Gao, H. Yang, and T. Li, "A wide-beam antenna for wide-angle scanning linear phased arrays," *IEEE Antennas Wireless Propag. Lett.*, vol. 19, no. 12, pp. 2122–2126, Dec. 2020.



Kun Wang received the B.S. degree in electronic and information engineering from the Hi-Tech College, Xi'an University of Technology, Xi'an, China, in 2012, and the M.S. degree in electronic and communication engineering from Shanghai Jiao Tong University, Shanghai, China, in 2017, where he is currently pursuing the Ph.D. degree in electromagnetic and microwave technology.

His current research interests include microstrip antennas, reconfigurable antennas, and millimeter-wave antennas.



Junping Geng (Senior Member, IEEE) received the B.S. degree in plastic working of metals, the M.S. degree in corrosion and protection of equipment, and the Ph.D. degree in circuit and system from Northwestern Polytechnic University, Xi'an, China, in 1996, 1999, and 2003, respectively.

From 2003 to 2005, he was a Post-Doctoral Researcher with Shanghai Jiao Tong University, Shanghai, China. In 2005, he joined the faculty of the Electronic Engineering Department, Shanghai Jiao Tong University, where he is currently an Associate Professor. From 2010 to 2011, he was a Visiting Scholar with the Institute of Electrical and Computer Engineering, University of Arizona, Tucson, AZ, USA. He has authored or coauthored over 300 refereed journal articles and conference papers, four books, and three book chapters. He holds over 90 patents with over 60 pending. He has been involved with multiantenna as for terminals, smart antennas, phase-mode antennas, generalized arrays, and nanoantennas. His main research interests include antennas, electromagnetic theory, computational techniques of electromagnetic, and nanoantennas.

Dr. Geng is a member of the Chinese Institute of Electronics (CIE) and a Committee Member of the Chinese antenna Society. He is also the Editor-in-Chief of the *Modern Antenna* (book series published by Springer in 2021). He was a recipient of the Technology Innovation Award from the Chinese Ministry of Education in 2007 and the Technology Innovation Award from the Chinese Government in 2008.



Han Zhou received the B.S. degree in information engineering from Shanghai Jiao Tong University, Shanghai, China, in 2014, where he is currently pursuing the Ph.D. degree in electromagnetic and microwave technology.

His current research interests include metamaterials, microwave devices, millimeter-wave phased array, and spoof surface plasmon polaritons' (SSPPs) antennas.



Silei Yang received the B.S. degree in electronic information engineering from the Anhui University of Finance and Economics, Bengbu, China, in 2017, and the M.S. degree in electronic science and technology from Shanghai Jiao Tong University, Shanghai, China, in 2020, where he is currently pursuing the Ph.D. degree.

His current research interests include spoof surface plasmon polaritons (SSPPs) antennas, microstrip antennas, and RF circuits.



Rui Zhao received the B.S. degree in electronic information engineering and the M.S. degree in electronic science and technology from the University of Electronic Science and Technology of China, Chengdu, China, in 2018 and 2021, respectively. She is currently pursuing the Ph.D. degree with Shanghai Jiao Tong University, Shanghai, China.

Her current research interests include spoof surface plasmon polaritons' (SSPPs) antennas, reconfigurable antennas, and wide-angle scanning arrays.



Jie Chen received the Ph.D. degree in computer architecture from the Huazhong University of Science and Technology, Wuhan, China, in 2014.

He is currently a Senior Engineer with the China Ship Development and Design Center (CSDDC), Wuhan, China. His current research interests include the integration of shipborne electronic information systems, reliability of distributed systems, and cloud computing.



Jingzheng Lu received the B.S. degree in electronic engineering from Xidian University, Xi'an, China, in 2020. He is currently pursuing the Ph.D. degree with the Department of Electronic Engineering, Shanghai Jiao Tong University, Shanghai, China.

His research interests include multibeam antennas, leaky-wave antennas, and spoof surface plasmon polaritons' (SSPPs) antennas.



Xudong Tang received the B.S. degree from Xidian University, Xi'an, China, in 2021. He is currently pursuing the Ph.D. degree in electronic science and technology with Shanghai Jiao Tong University, Shanghai, China.

His current research interests include phase antenna, polarization reconfigurable antenna, and spoof surface plasmon polaritons' (SSPPs) antennas.



Jing Zhang received the B.S. degree in communication engineering from Wuhan University, Wuhan, Hubei, China, in 2019, and the M.S. degree in electronic and communication engineering from Shanghai Jiao Tong University, Shanghai, China, in March 2022.

Her research interests include microstrip antennas, spoof surface plasmon polaritons' (SSPPs) antennas, and array.



Ronghong Jin (Fellow, IEEE) received the B.S. degree in electronic engineering, the M.S. degree in electromagnetic and microwave technology, and the Ph.D. degree in communication and electronic systems from Shanghai Jiao Tong University (SJTU), Shanghai, China, in 1983, 1986, and 1993, respectively.

In 1986, he joined the Department of Electronic Engineering, SJTU, where he was an Assistant, a Lecturer, and an Associate Professor and is currently a Professor. From 1997 to 1999, he was a Visiting Scholar with the Department of Electrical and Electronic Engineering, Tokyo Institute of Technology, Meguro, Japan. From 2001 to 2002, he was a Special Invited Research Fellow with the Communication Research Laboratory, Tokyo, Japan. From 2006 to 2009, he was a Guest Professor with the University of Wollongong, Wollongong, NSW, Australia. He is also a Distinguish Guest Scientist with the Commonwealth Scientific and Industrial Research Organization, Sydney, NSW, Australia. He has authored or coauthored over 400 papers in refereed journals and conference proceedings and coauthored seven books. He holds more than 70 patents in antenna and wireless technologies. His current research interests include antennas, electromagnetic theory, numerical techniques for solving field problems, and wireless communications.

Dr. Jin is a Committee Member of the Antenna Branch of the Chinese Institute of Electronics, Beijing, China. He was a recipient of the National Technology Innovation Award, the National Nature Science Award, the 2012 Nomination of National Excellent Doctoral Dissertation (Supervisor), the 2017 Excellent Doctoral Dissertation (Supervisor) of the China Institute of Communications, the Shanghai Nature Science Award, and the Shanghai Science and Technology Progress Award.